Influence of Shielding on Conducted EMI in High-Power Wireless Power Transfer Systems

Mattia Simonazzi, *Member, IEEE*, Vincenzo Cirimele, *Senior Member, IEEE*, Riccardo Mandrioli, *Senior Member, IEEE*, and Leonardo Sandrolini, *Senior Member, IEEE*

***Abstract*—Wireless power transfer (WPT) systems are widely used in automotive and consumer electronics due to the many benefits they can offer. However, according to the inherent presence of power electronics and extended electromagnetic parts, they can be the source of significant electromagnetic interference (EMI). This paper investigates the conducted emissions (CEs) of a 1 kW WPT system, assessing the effect of the conductive shields of the coil assemblies on the CEs through a purely experimental approach. The study also considers the effect of power modulation implemented by a phase-shift control and highlights its impact on the overall CE behavior. The objective is to provide a quantitative insight into the role of the shielding in WPT conducted emissions, considering both the conditions of grounded and ungrounded shields. The measurements are conducted over the DC bus of a GaN-based commercially available evaluation board in order to guarantee the highest level of reproducibility of the results. The CEs are measured with an EMI receiver and the impedance seen from the system under test to the power supply is stabilized with a line impedance stabilization network (LISN).**

***Index Terms*—Inductive power transmission, wireless power transfer, conducted emissions, EMC, EMI.**

I. Introduction

THE increasing penetration of wireless power transfer (WPT) systems in both the automotive and consumer electronics markets has inevitably drawn attention to the electromagnetic interference (EMI) challenges these systems inherently pose. The commercially viable WPT systems are typically of the kind indicated as inductive power transfer (IPT) [1], [2]. This is because, compared with other wireless power transfer systems that operate over limited distances, IPT systems allow for greater power density, robustness, and can be easily integrated into casings that can be installed in various application contexts. It is for these reasons that this technology has been adopted in a variety of areas, ranging from military to civilian applications such as electric vehicle charging in both automotive and industrial sectors [3], [4], [5], bio-medical [6], [7], and consumer electronics applications [8], [9].

IPT systems operate based on magnetic induction between two magnetically weakly coupled coils named the transmitter and the receiver. To compensate for this relatively low coupling, these systems are made resonant and, in the automotive field, operate at several tens or hundreds of kilohertz [1], [2]. The coils are accompanied by various spatially extended auxiliary elements such as ferrite plates or conductive shields, composing the so-called assemblies. These elements, which are introduced to guide and confine the magnetic field, inevitably introduce parasitic couplings with the ground and nearby metallic elements. These parasitic couplings create return paths for undesired currents, which lead to electromagnetic compatibility issues, and must therefore be identified, analyzed, and addressed from the design stage. It is for these reasons that the different standards developed with reference to IPT systems are introducing increasingly stringent electromagnetic compatibility (EMC) requirements [10], [11].

WPT for electric vehicles (EVs) sits at the intersection of general EMC rules and several automotive-specific standards. SAE J2954 is the primary industry specification addressing interoperability, electromagnetic emissions/immune limits for light-duty EVs [10], [11], [12]. For component-level radiated and conducted emissions testing, the automotive reference is CISPR 25, which sets measurement procedures and limits for radio disturbance from vehicle components across the relevant frequency range [13]. For industrial EV, reference has to be made to CISPR 11 [14]. UNECE Regulation no. 10 includes requirements for emissions and immunity for electric vehicles and their charging systems [15]. Immunity to radiated RF fields is also assessed based on IEC 61000-4-3, which is often applied alongside automotive test methods to verify WPT transmitter/receiver robustness to ambient fields [16].

However, despite the possibility of reference to various regulatory documents, this field still presents several open issues for

Received 19 November 2025; revised 28 January 2026; accepted 13 March 2026. Date of publication 23 March 2026; date of current version 17 April 2026. This work was supported in part by the National Recovery and Resilience Plan (NRRP); in part by the Mission 04 Component 2: Investment 1.3—Next Generation EU, PE2 - NEST—Network 4 Energy Sustainable Transition, under Grant PE00000021, Spoke 5 Energy Conversion, Spoke 6 Energy Storage, Spoke 7 Smart Sector Integration; in part by the Investment 1.5—Next Generation EU, ECOSISTER–Ecosystem for Sustainable Transition in Emilia-Romagna, under Grant ECS_00000033, Spoke 4 Smart Mobility Housing and Energy Solutions. The associate editor coordinating the review of this article and approving it for publication was Tommaso Campi. *(Corresponding author: Vincenzo Cirimele.)*

The authors are with the Department of Electrical, Electronic, and Information Engineering, University of Bologna, 40136 Bologna, Italy (e-mail: mattia.simonazzi2@unibo.it; vincenzo.cirimele@unibo.it; r.mandrioli@unibo.it; leonardo.sandrolini@unibo.it).

Digital Object Identifier 10.1109/JWPT.2026.3676524

© 2026 The Authors. This work is licensed under a Creative Commons Attribution-NonCommercial-NoDerivatives 4.0 License.
for more information. see https://creativecommons.org/licenses/by-nc-nd/4.0/

IPT systems. Indeed, even if IPT systems have been widely analyzed under different aspects, there is still a notable lack of research addressing their behaviour and design from the point of view of the electromagnetic compatibility aspects. At present and to the best of the author's knowledge, only a few works have investigated conducted emissions (CEs) in IPT systems [11], [17], [18], [19], [20], [21]. More specifically, these works mainly address DC CEs despite the fact that the EMC regulations referenced by the standards on WPT mainly address CEs in the AC network. This is due to the fact that DC disturbances are directly related to the operation of the WPT system's main components (i.e., the DC/AC converter that supplies the transmitter coil through its compensation network), while the AC CEs are mainly influenced by devices connected upstream of the inverter DC bus (i.e., active or passive rectifiers). Then, DC CEs can be effectively mitigated through design interventions, such as limiting cross-talk effects in PCBs and selecting appropriately characterized components with moderate parasitics.

In this frame, a general study on the conducted and radiated emissions of an SAE J2954-compliant WPT system with measurements is presented in [11]. This work considers EMC tests on a 3.6 kW prototype with a main focus and discussion on the EMI filter design. Specific studies focusing on DC CEs are presented in [18], where the DC CEs of a WPT system with air-core coils are characterized for different alignment conditions and in [21], where the CEs with different compensation strategies are discussed. In [19] and [20], special power electronics and related control strategies are presented to mitigate DC CE emissions. These studies focus on the analysis of emissions at the system level for prototypes, and the role of individual system components is discussed only in [21] terms of compensation networks.

The present article, which is an extension of the work [22], is intended to be an initial contribution to fill the gap in the literature on the detailed characterization of CEs. It presents a purely experimental analysis of the conducted emissions of a high-power IPT system with the aim of investigating the impact of shielding systems on the levels of conducted emissions. A comparison is performed by assessing the DC CEs for WPT assemblies in the presence or absence of the conductive shield at both the transmitter and receiver sides. Moreover, the grounding of the transmitter-side shield, usually performed for electrical safety reasons, is also analysed. For each of these configurations, the conducted emissions have also been analysed under power modulation conditions implemented through the phase-shift control technique, which is commonly used in the regulation of WPT systems for automotive and industrial applications [23], [24], [25]. The DC/AC converter used to supply the transmitter coil consists of an H-bridge formed by connecting two GaN-based Infineon half-bridge evaluation boards in parallel. This choice allows the use of extremely simple circuitry, based on a few components and without filters on the DC side other than a single electrolytic filter capacitor. This design enables extreme control of the device and its modeling and, at the same time, guarantees the highest possible reproducibility of results, as the layouts and all components of the boards used are completely publicly accessible [26].

The remainder of the manuscript is organized as follows. Section II introduces the WPT system under consideration as well as three comparative cases. Experimental results are collected and discussed in Section III. Section IV draws conclusions.

II. WPT Systems Under Test

The WPT system considered in this work consists of a transmitting coil, referred to as Tx, and a receiving coil, denoted as Rx. The transmitter comprises a circular coil with an external diameter of 19 cm, consisting of 18 turns distributed across two layers made of litz wire with a cross-section of 4 mm^2. The receiver consists of a circular coil with an external diameter of 15 cm, featuring 6 turns made of litz wire with a cross-section of 10 mm^2. Both coils are placed on a square 3C94 ferrite plate with a side length of 20 cm and a thickness of 5 mm. The distance between Tx and Rx coils is set to a nominal value of 8 cm.

A series-series compensation is used, realized with two capacitor banks referred to as C_1 and C_2, designed to make the system resonate at $f_0 = 85$ kHz as suggested by the automotive standards [10]. The load R_l has been chosen based on the desired power rating.

The system has been designed so that the transmitter and receiver quality factors meet the constraints

$$Q_1 > 4 \quad \text{and} \quad Q_1 > \frac{4Q_2^3}{4Q_2^2 - 1}, \tag{1}$$

to ensure the absence of bifurcation and guarantee a negligible deviation from the sinusoidality of the current supplied by the source [27], [28]. Q_1 and Q_2 are defined as

$$Q_1 = \frac{R_l L_1}{\omega_0 M^2}, \tag{2}$$

$$Q_2 = \frac{\omega_0 L_2}{R_l}, \tag{3}$$

with $\omega_0 = 2\pi f_0$.

The self-inductance values of the transmitter L_1 and receiver L_2, as well as their mutual inductance M, have been preliminarily assessed through numerical simulations conducted using the commercial software COMSOL Multiphysics, which is based on the finite element method. The obtained values are $L_1 = 138$ μH, $L_2 = 15$ μH, $M = 8.35$ μH.

The source supplying the system is an H-bridge, implemented using two Infineon half-bridges based on GaN technology [26] and controlled by a signal generator. The signal generator is used to emulate a phase-shift modulation, which is the most widely adopted modulation technique to control the value of the output voltage $v_1(t)$ of the H-bridge (see Fig. 1) [23], [24], [25]. The rms value of this voltage, indicated as V_1, is controlled via a shift angle α on the basis of the following equation:

$$V_1 = \frac{2\sqrt{2}}{\pi} V_{DC} \cdot \cos\left(\frac{\alpha}{2}\right) \tag{4}$$

where α is the shifting electrical angle between the gate signals of the two half-bridges. To ensure zero-voltage switching operations under full square wave output voltage (i.e. $\alpha = 0$), the switching frequency of the converter is tuned so that the input

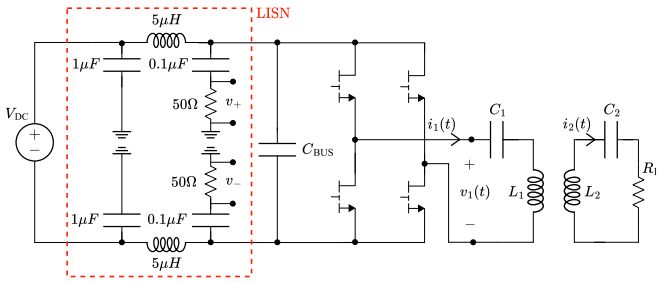

Fig. 1. Schematic of the WPT system with the upstream LISNs for CE measurements.

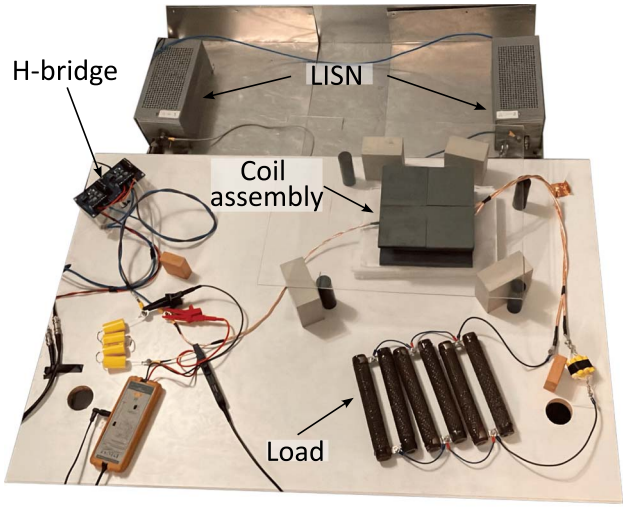

(a) Whole WPT system under CASE 1

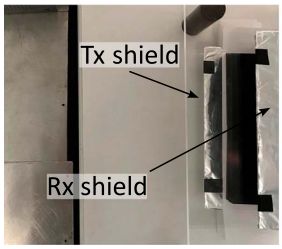

(b) CASE 2 shield

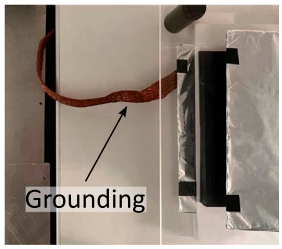

(c) CASE 3 shield

Fig. 2. Experimental setup of the WPT system under test.

impedance of the coupling network (measured at the inverter output port) presents a slightly inductive behavior [29].

Conducted emissions have been measured using an R&S ESRP EMI receiver and a line impedance stabilization network (LISN), connected between the power supply and the inverter DC bus as depicted in Fig. 1. The use of the LISN allows the decoupling of the power source from the system under test within the frequency range of emission measurements, that is, the range 150 kHz – 30 MHz. The EMI receiver processes the disturbance signals v_+ and v_- acquired at the measurement ports of the LISN (see Fig. 1). The experimental setup is shown in Fig. 2(a).

A. Shielding WPT Systems

Existing standards (e.g., SAE J2954) indicate the use of a ferrite plate near the coils in both the ground assembly (GA) and

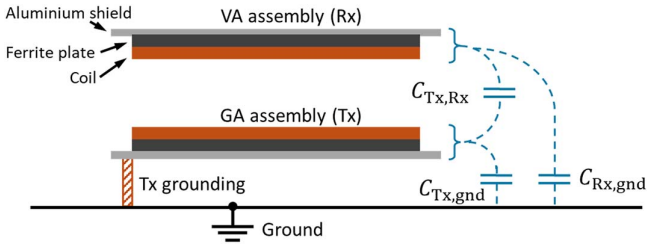

Fig. 3. Schematic illustration of the considered WPT system with parasitic capacitances. The possible grounding of the Tx assembly is also depicted.

vehicle assembly (VA), along with 2 mm thick aluminium shields. Ferrite materials are commonly employed to guide the magnetic flux in the proximity of the coils to increase the magnetic coupling. Together with the ferromagnetic plate, the example designs included in the standards recommend the use of conductive shields on both sides. These conductive shields can reflect or absorb the electromagnetic field. The combination of these two materials helps in minimizing the leakage fields that can illuminate and interact with devices or general metallic objects in the proximity of the WPT system.

However, improper shielding design can lead to undesired resonances, eddy currents, or impedance mismatches, which may increase conducted EMI. The electrical conductivity of these materials, particularly of the aluminium adopted for the conductive shielding, can play a crucial role in defining the return path of disturbance currents. These currents are significantly influenced by the system's parasitic elements, such as unwanted electrical and magnetic couplings between system components and the ground.

A schematic representation of the capacitive coupling mechanisms in the analyzed system is provided in Fig. 3. The figure highlights the parasitic capacitances that arise due to the electrical conductivity of the materials and their mutual coupling, including coupling to ground. The value of these capacitances is highly dependent on the relative distances between objects and the ground, and is typically in the picofarad to hundreds of picofarad range [30]. These capacitances can create high-frequency unintended return paths for disturbance currents, allowing their circulation and thereby generating unwanted interference that propagates back toward the source.

Depending on the installation methods and accessibility of the Tx assembly, common electrical safety practices may suggest connecting the conductive shields to ground as shown in Fig. 3. This connection has an effect on the capacitances shown in the figure and therefore involves a change in the disturbance currents return paths.

To analyze these effects, a purely experimental approach is adopted in this study, as real-world systems exhibit many complex, non-ideal, and application-dependent behaviors that are difficult to model and generalize. Empirical validation instead allows for direct assessment of shielding impact under practical conditions, capturing phenomena such as coupling effects, common-mode noise, and differential-mode noise that may not be fully predictable through simulations alone.

The shields used for both the transmitter and receiver coils consist of 30 cm × 30 cm aluminium plates, positioned beneath

TABLE I
MEASURED VALUES OF SETUP MAIN COMPONENTS

Parameter	Symbol	Value	Unit
Tx inductance	L_1	136	μH
Rx inductance	L_2	14.6	μH
Tx capacitance	C_1	24.6	nF
Rx capacitance	C_2	188	nF
DC-bus capacitance	C_{BUS}	204	μF
Load resistance	R_l	2.30	Ω
Load parasitic inductance	ESL	4.70	μH

the ferrites. A thin sheet of paper is inserted to ensure electrical insulation between the ferrites and the aluminium plates.

As visible in Fig. 2(a), a connection was established between the LISN ground plane and the transmitter shield using a 7 cm wide copper braid, ensuring a low-impedance connection.

This study aims to provide quantitative insights into the role of shielding in WPT systems, showing the behavior of the conducted emission in three different situations:

- CASE 1: Absence of shields (see Fig. 2(a)). In this case, only the ferrite plates are present.
- CASE 2: Aluminium shields on both Tx and Rx sides (see Fig. 2(b)).
- CASE 3: Aluminium shield on both Tx and Rx sides with grounding of the Tx shield (see Fig. 2(c)).

III. EXPERIMENTAL RESULTS

As visible in Fig. 2(a), the system load is created by connecting six wirewound power resistors in parallel. These resistors exhibit significant parasitic inductances, which can consequently modify the overall inductance of the receiver side of the system. Therefore, the whole resistive load, as well as the coils, were characterized by means of an impedance measurement using an LCR bridge at the frequency of 85 kHz, which is the rated operating frequency (i.e. the resonance frequency of the system) indicated by the standards for automotive applications [10]. The receiver-side compensation capacitors were therefore chosen to compensate for both the self-inductance of the coil and the parasitic inductance of the resistive load at the resonance frequency. The results of the measurements and the main system parameters are summarized in Table I.

The measured inductance values were found to closely match the estimated design values indicated in Section II. Clearly, these values varied slightly depending on the presence or absence of conductive shields, leading to a small shift in the resonance frequency. To compensate for this effect, the operating frequency of the H-bridge was adjusted to maintain the same phase of the system input impedance. The effect on the mutual inductance was instead found to be negligible, so no corrections on the coil distance were necessary to ensure that the transferred power remained at around 1 kW in the rated working conditions, i.e., at the resonance frequency and $\alpha = 0$. The power values remain clearly closely matched also in the other phase shifting conditions analyzed, as shown in Table II. It is possible to see how the actual operating frequency was adjusted in the different cases to maintain the same operating conditions (i.e., phase and amplitude of the impedance of the system under test), but how the value always remained within the range 79 kHz – 90 kHz indicated by the SAE J2954 standard and other international standards on WPT for light-duty EVs [10], [12]. The values of the input voltage V_{DC} and the input power P_{in} were directly read from the DC power supply adopted as the DC source.

TABLE II
MEASURED RESONANCE FREQUENCY AND POWER AT EACH PHASE-SHIFTING CONDITION

α (rad)	f_0 (Hz)	V_{DC} (V)	P_{in} (W)
CASE 1			
0	87.0	110.0	1112
$\pi/4$	87.0	110.0	1064
$\pi/3$	87.0	110.0	968.0
$\pi/2$	87.0	110.0	794.2
$2\pi/3$	87.0	110.0	477.1
CASE 2 and CASE 3			
0	89.5	110.0	1157
$\pi/4$	89.5	110.0	1103
$\pi/3$	89.5	110.0	902.6
$\pi/2$	89.5	110.0	552.1
$2\pi/3$	89.5	110.0	533.1

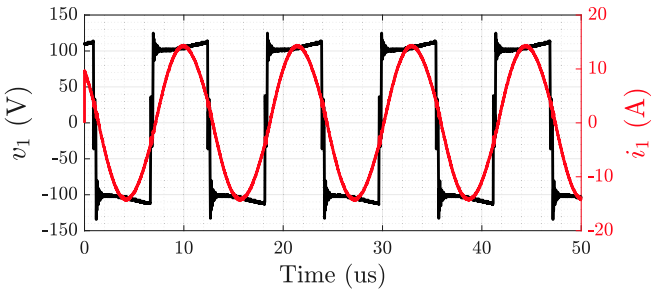

(a) CASE 1

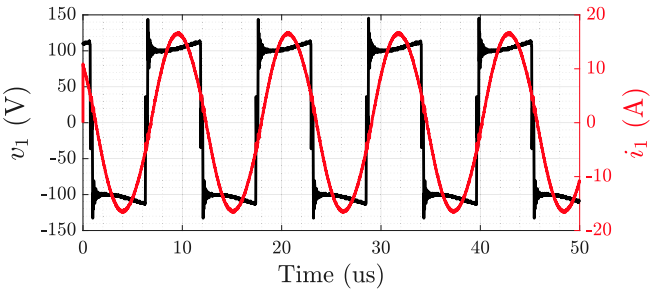

(b) CASE 2 and 3

Fig. 4. Input voltage (black) and current (red) waveforms with $\alpha = 0$, which gives the full (square) voltage wave.

The voltage $v_1(t)$ and current $i_1(t)$ waveforms at the input of the coupling system in the three different configurations CASE 1, CASE 2 and CASE 3 are shown in Figs. 4, 5 and 6 for $\alpha = 0$, $\alpha = \pi/2$ and $\alpha = 2\pi/3$, respectively. The analysis of these waveforms reveals that the voltage profile remains nearly unchanged across all three configurations (referred to as cases), indicating that the presence of the shield does not significantly affect the voltage characteristics at the system input.

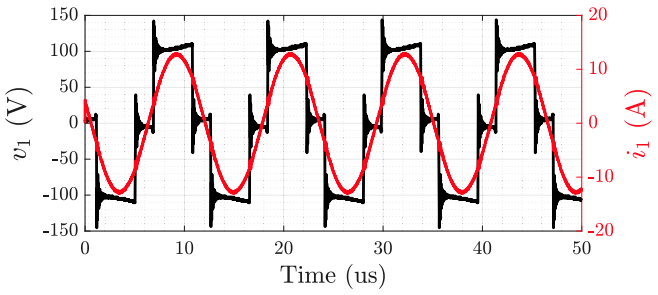

(a) CASE 1

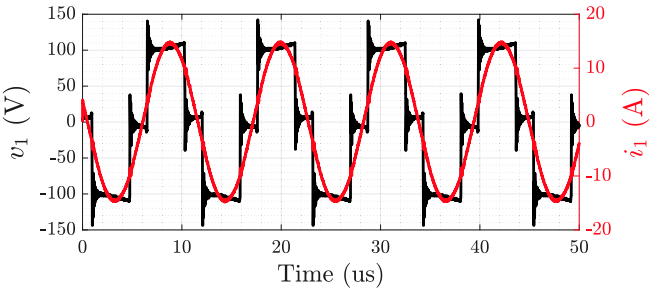

(b) CASE 2 and 3

Fig. 5. Input voltage (black) and current (red) waveforms with $\alpha = \pi/2$.

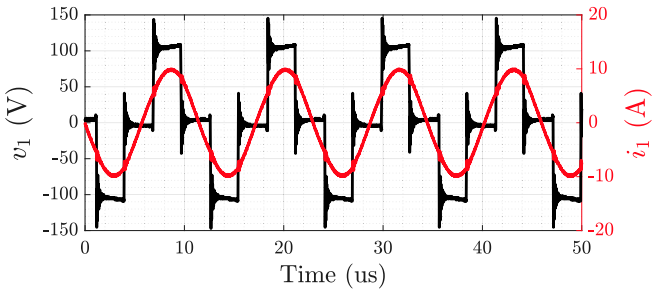

(a) CASE 1

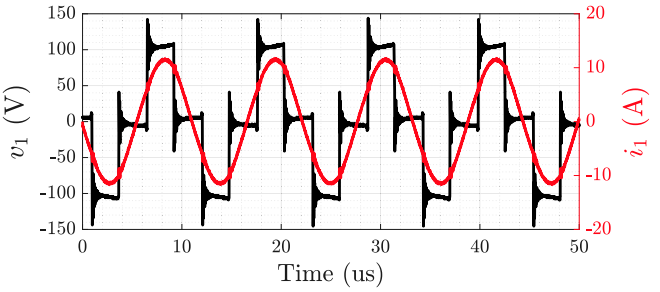

(b) CASE 2 and 3

Fig. 6. Input voltage (black) and current (red) waveforms with $\alpha = 2\pi/3$.

As already mentioned, the operating frequency of the system in CASES 1, 2, and 3 was specifically adjusted to ensure resonance, and the tuning was performed in the condition $\alpha = 0$. From Fig. 4, it can be observed that the current waveform exhibits a slight reduction in the amplitude and a slight increase in the operating frequency became necessary to ensure the leading phase shift (i.e., slightly inductive behavior). This indicates how the shielding tends to lower the imaginary part of the input impedance, slightly impacting the current waveform, while leaving the voltage largely unaffected. Grounding the transmitter shield does not introduce any further modifications to the voltage and current waveforms at the inverter input, confirming that the power transfer of the system remains stable regardless of this specific grounding condition. For this reason, in Figs. 4–6 the plot for CASE 2 is reported as representative for CASE 3, too.

In all tested scenarios, the current waveform shows a slight lag, proving the slightly inductive nature of the system input impedance. This testifies the feasibility of soft-switching operation for the inverter, suggesting that the presence of the shield, while slightly affecting the phase and amplitude of the current, does not compromise the overall system performance.

The phase shift can be appreciated from Figs. 5 and 6, where the voltage waveform appears modulated, exhibiting an additional level, corresponding to a reduced duty cycle. However, since the fundamental component of the voltage is tuned to the resonance frequency of the series–series compensated WPT system, and the coils are designed to respect Eq. 1, the resulting current remains purely sinusoidal. The voltage modulation indeed controls the transferred power without deteriorating the coil currents' harmonic purity.

A. CE of the Phase-Shift Controlled WPT System

The measurements of conducted emissions in the 150 kHz – 30 MHz frequency range are shown for the three different cases and different α in Figs. 7 and 8. In the figures, the limits specified in the UNECE R10 standard are shown for a comparative reference. It is clearly important to recall that the DC/AC converter adopted does not include any EMC filter. Consequently, these limits do not serve to verify compliance but are reported exclusively for the purpose of providing a common quantitative basis for comparison. It is also important to emphasise that the limits given in the standard refer to quasi-peak values, whereas the reported spectra correspond to peak values. As expected, the highest disturbance is observed at lower frequencies and, in particular, a fundamental frequency component can be identified at twice the system operating frequency f_0, this latter corresponding to the switching frequency of the inverter.

The filtering effect of the DC bus, which primarily depends on the capacitance value and parasitic parameters such as resistance and inductance, determines the spectral characteristics of the resulting interference. As previously discussed, the introduction of shielding slightly modifies the current waveform, as it affects the system impedance to some extent. This change can, in turn, influence the spectral characteristics of the conducted emissions. In CASE 1, the operating frequency is chosen slightly lower than the ones in CASEs 2 and 3 to compensate for the shield effect on the input impedance. This can be appreciated from the shift of the first peak (which is the highest) in the CE spectra of Fig. 7.

It is well known that in the mid-to-high frequency range of the spectrum, common-mode noise becomes dominant [31]. These disturbances arise from currents that return to ground through parasitic couplings, which are highly dependent on the specific layout of the system. These parasitic effects are particularly challenging to predict, as they are influenced by electrical

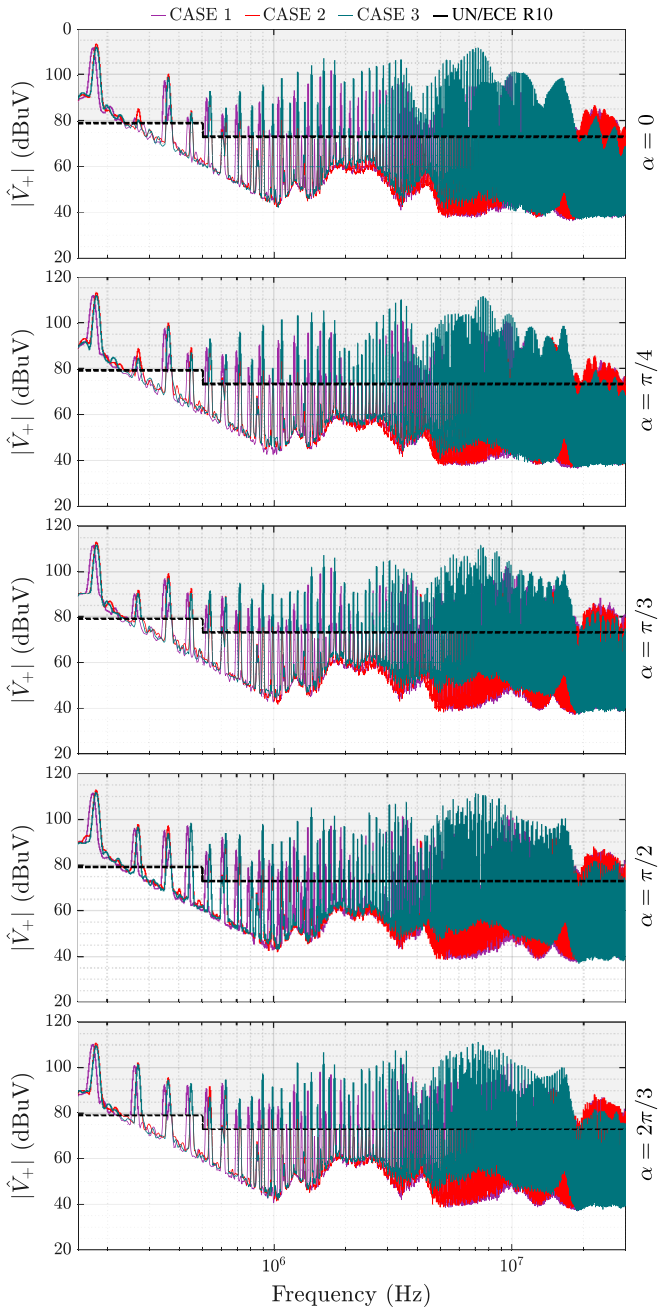

Fig. 7. CE pectra for different α values.

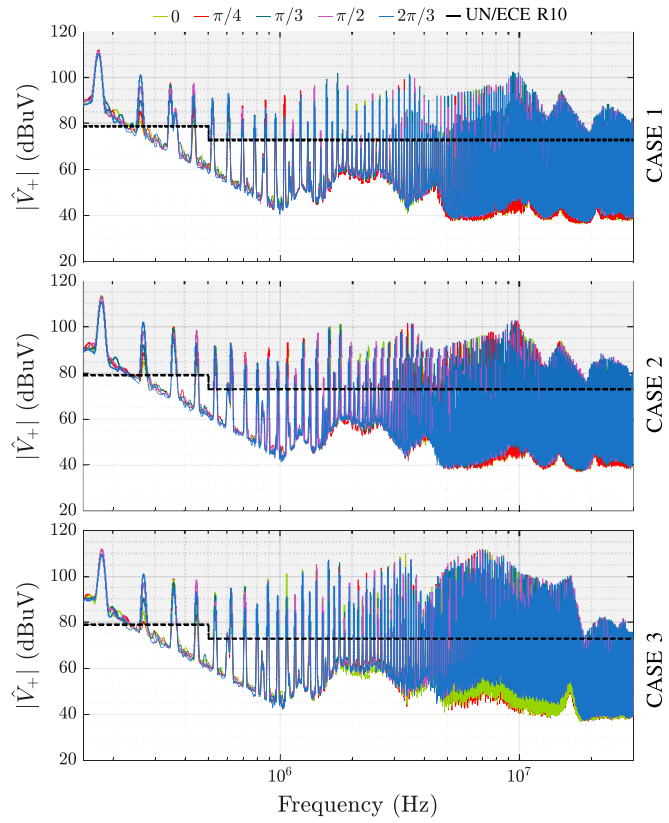

Fig. 8. CE spectra in the three different cases.

couplings and the presence of conductive elements, which play a crucial role in shaping the system's electromagnetic behavior. From Fig. 7, it can be noticed no appreciable variation of the CEs between CASE 2 (with the introduction of shielding) and CASE 1. A significant deterioration is instead observed when the transmitter-side shield is grounded, i.e., CASE 3. The grounding drastically increases the CE in the range 1 MHz – 10 MHz compared to CASE 1 and CASE 2, while leading to a significant reduction of approximately 35 dBµV around 20 MHz.

The introduction of a phase shift in the modulation results in the emergence of additional harmonic components. These components are particularly pronounced at low frequencies, i.e., in the range below 1 MHz) typically associated with differential-mode conducted emissions. This observation is evident when comparing the results to those obtained in the absence of phase-shifting (i.e., Fig. 7 $\alpha = 0$) with those at $\alpha = \pi/2$ and $\alpha = 2\pi/3$. The presence of the shielding and its grounding does not significantly alter this trend: for each configuration, the spectral variation consistently follows the same evolution according to the phase-shift angle α (continue to make reference to Fig. 7).

While in the case $\alpha = 0$ the low-frequency spectrum is dominated by even harmonics, originating from the rectified sine-wave behavior at the H-bridge DC bus, the additional harmonics appearing in the presence of phase-shifting are odd multiples of the fundamental (i.e., switching) frequency f_0. The transmitter current $i_1(t)$ remains perfectly sinusoidal due to the filtering effect of the resonant network. Therefore, the appearance of these harmonics can be attributed to the altered shape of the primary voltage $v_1(t)$ and to the specific combination of switch commutations, which allows the circulation of more distorted disturbance currents at the inverter input. This behavior highlights the strong correlation between the shift angle and the spectral distribution of the transmitter voltage and current, which in turn influences the overall electromagnetic emission profile of the WPT system at low frequency (i.e., below 1 MHz).

For each of the three cases, the effect of the phase shifting on the CE spectra can be appreciated from Fig. 8. For each of these spectra, it can be observed that the odd harmonic components of the fundamental progressively increase with the phase-shift angle α. It is worth noting, however, that some exceptions occur for the components at $5f_0$ and $13f_0$, which reach their maximum

amplitude at $\alpha = \pi/2$. Although these dynamics are primarily governed by the modulation scheme and operating conditions, they are also strongly influenced by the current return paths and the circuit topology. The impact of all these interacting components is not straightforward to predict, either numerically or analytically.

As the frequency increases, the harmonic components tend to propagate through parasitic couplings to ground, making it difficult to describe their exact behavior at higher frequencies, unlike what can be done for the lower-frequency components. In particular, when the shield is added without grounding, the spectral characteristics remain almost unchanged. Conversely, grounding the transmitter-side shield leads to a significant increase in conducted emissions, especially in the frequency band above 1 MHz. In particular, an increase of approximately 16 dBμV is observed around 8 MHz, from 96 dBμV to 112 dBμV. Finally, a drastic reduction in conducted emissions is again observed in the region around 20 MHz, confirming the spectral behavior previously discussed.

It can be concluded that at higher frequencies, the spectral content is only marginally affected by the modulation itself and is instead mainly determined by the system layout, particularly by the presence and grounding configuration of the shielding.

IV. Conclusion

In this paper, the DC conducted emissions of a 1 kW WPT system have been assessed in three different configurations: without shielding (CASE 1), with shielding (CASE 2), and with shielding where the transmitter-side shield is grounded (CASE 3). Overall, it can be stated that the presence of shielding does not significantly alter the CE spectrum compared to CASE 1. However, grounding the transmitter-side shield increases conducted emissions in the mid-frequency range while reducing them at higher frequencies. Given the considerable increase (approximately 10 dBμV) in conducted noise voltage in CASE 3 compared to CASES 1 and 2, this grounding configuration may pose a potential issue in terms of electromagnetic compatibility.

The necessity to regulate the transferred power by introducing a phase shift on the gate signals of the H-bridge can introduce additional spectral distortion, leading to the appearance of odd harmonics whose amplitude increases with the phase-shift angle between the H-bridge legs. This effect is particularly evident at low frequencies, within the range dominated by differential-mode disturbances, whereas at higher frequencies (above approximately 10 MHz), the modulation does not significantly alter the harmonic amplitudes, although harmonics of different orders may appear depending on the selected modulation angle.

The experimental results demonstrate that the shield-to-coil and shield-to-ground capacitances, together with the grounding configuration of the transmitter coil shield, play a fundamental role in shaping common-mode noise. The influence of these couplings shows only a weak dependence on the modulation technique adopted for the power converter. Nevertheless, a very limited mitigation can be achieved by employing modulation strategies that limit voltage partialization during power transfer regulation.

While the magnitude of the effects varies with the specific geometric implementation of the system, the observed correlations and emission trends remain consistent and are therefore applicable beyond the particular setup investigated. Therefore, the results provide useful guidance for the management of shielding and grounding strategies, as well as for the preliminary sizing of EMC filters.

Overall, the findings indicate that shield grounding—often imposed by higher-level protection and safety requirements—naturally leads to increased emission levels. Whenever safety regulations allow, avoiding direct grounding of the shield emerges as the most effective approach to reduce high-frequency common-mode conducted noise. When shield grounding is mandatory, mitigation efforts should focus on the power interface rather than on modifications to the shield itself. Although the selection of component values and layout details remains application-dependent and follows standard EMC design practices, the preliminary design of mitigation filters can be effectively informed by the results presented in this work.

References

[1] G. A. Covic and J. T. Boys, "Modern trends in inductive power transfer for transportation applications," *IEEE J. Emerg. Sel. Topics Power Electron.*, vol. 1, no. 1, pp. 28–41, Mar. 2013.

[2] V. Cirimele, M. Diana, F. Freschi, and M. Mitolo, "Inductive power transfer for automotive applications: State-of-the-art and future trends," *IEEE Trans. Ind. Appl.*, vol. 54, no. 5, pp. 4069–4079, Sep. 2018.

[3] O. C. Onar, M. Chinthavali, S. L. Campbell, L. E. Seiber, and C. P. White, "Vehicular integration of wireless power transfer systems and hardware interoperability case studies," *IEEE Trans. Ind Appl.*, vol. 55, no. 9, pp. 5223–5234, Sep.–Oct. 2019.

[4] M. Simonazzi, A. Campanini, L. Sandrolini, and C. Rossi, "Single stage wireless power transfer battery charger for electric vehicles," in *Proc. IEEE 15th Int. Conf. Compat. Power Electron. Power Eng. (CPE-POWERENG)*, 2021, pp. 1–6.

[5] A. Faveto, L. Panza, G. Bruno, V. Cirimele, S. S. Furio, and F. Lombardi, "Efficient management of industrial electric vehicles by means of static and dynamic wireless power transfer systems," *Int. J. Adv. Manuf. Technol.*, vol. 123, no. 3, pp. 1249–1267, 2022.

[6] A. Iqbal, P. R. Sura, M. Al-Hasan, I. B. Mabrouk, and T. A. Denidni, "Wireless power transfer system for deep-implanted biomedical devices," *Scientific Rep.*, vol. 12, no. 1, 2022, Art. no. 13689.

[7] S. Ding, S. Koulouridis, and L. Pichon, "Miniaturized implantable power transmission system for biomedical wireless applications," *Wireless Power Transfer*, vol. 7, no. 1, pp. 1–9, 2020.

[8] X. Yu, J. Feng, L. Zhu, and Q. Li, "Design and optimization of a planar omnidirectional wireless power transfer system for consumer electronics," *IEEE Open J. Power Electron.*, vol. 5, pp. 311–322, 2024.

[9] L. Zhao, X. Chen, J. Xiao, V. Cirimele, H. Hu, and P. A. Hu, "A high power density and nearly constant voltage WPT system based on bendable PCB," *IEEE Trans. Ind. Electron.*, vol. 72, no. 12, pp. 14931–14936, Dec. 2025.

[10] V. Cirimele, F. Freschi, and L. Zhao, "Critical comparative review of international standards on wireless charging for light-duty electric vehicles," *IEEE Trans. Ind. Appl.*, vol. 60, no. 5, pp. 7403–7412, Sep.–Oct. 2024.

[11] E. Sulejmani, M. Beltle, and S. Tenbohlen, "EMC of inductive automotive charging systems according to standard SAE J2954," *Vehicles*, vol. 5, no. 4, pp. 1532–1552, 2023.

[12] Society of Automotive Engineers, *Wireless Power Transfer for Light-Duty Plug-in/Electric Vehicles and Alignment Methodology*, SAE J2954_202408, 2024. Accessed: Mar. 20, 2026. [Online]. Available:

https://www.sae.org/standards/j2954_202408-wireless-power-transfer-light-duty-plug-electric-vehicles-alignment-methodology
[13] Comité international spécial des perturbations radioélectriques, *Vehicles, Boats and Internal Combustion Engines - Radio Disturbance Characteristics - Limits and Methods of Measurement for the Protection of on-Board Receivers*, CISPR 25, 2022. Accessed: Mar. 20, 2026. [Online]. Available: https://webstore.iec.ch/en/publication/64645
[14] Comité international spécial des perturbations radioélectriques, *Industrial, Scientific and Medical Equipment - Radio-Frequency Disturbance Characteristics - Limits and Methods of Measurement*, CISPR 11, 2024. Accessed: Mar. 20, 2026. [Online]. Available: https://webstore.iec.ch/en/publication/66118
[15] United Nations, "Uniform provisions concerning the approval of vehicles with regard to electromagnetic compatibility (UN Regulation No. 10, Revision 6)". [Online]. Available: https://eur-lex.europa.eu/legal-content/EN/TXT/PDF/?uri=CELEX:42017X0260
[16] International Electrotechnical Commission, *Electromagnetic Compatibility (EMC) - Part 4-3 : Testing and Measurement Techniques - Radiated, Radio-Frequency, Electromagnetic Field Immunity Test*, IEC 61000-4-3:2020. Accessed: Mar. 20, 2026. [Online]. Available: https://webstore.iec.ch/en/publication/59849
[17] J. Alberto, U. Reggiani, and L. Sandrolini, "Study of the conducted emissions of an IPT system composed of an array of magnetically coupled resonators," in *Proc. IEEE Int. Symp. Electromagn. Compat. Signal/Power Integrity (EMCSI)*, 2017, pp. 623–628.
[18] M. Simonazzi and L. Sandrolini, "Conducted emission analysis of a near-field wireless power transfer system," in *Proc. IEEE 15th Int. Conf. Compat. Power Electron. Power Eng.*, 2021, pp. 1–6.
[19] L. Zhai, Y. Cao, L. Lin, T. Zhang, and S. Kavuma, "Mitigation conducted emission strategy based on transfer function from a DC-fed wireless charging system for electric vehicles," *Energies*, vol. 11, no. 3, p. 477, Feb. 2018.
[20] D. Stepins, J. Zakis, J. Audze, O. Husev, B. Pakhaliuk, and V. Shevchenko, "Reduction of conducted emissions generated by WPT systems with multilevel inverters using spread spectrum approach," in *Proc. 46th Annu. Conf. IEEE Ind. Electron. Soc.*, 2020, pp. 3924–3929.
[21] T. Campi, S. Cruciani, F. Maradei, and M. Feliziani, "Conducted emission of wireless power transfer charging system in electric vehicle," in *Proc. IEEE Int. Symp. Electromagn. Compat. Signal/Power Integrity*, Washington, DC, USA, 2017, pp. 619–622.
[22] M. Simonazzi, V. Cirimele, R. Mandrioli, and L. Sandrolini, "Shielding impact on conducted emission of a kW-level WPT system: An experimental approach," in *Proc. IEEE Wireless Power Technol. Conf. Expo (WPTCE)*, Piscataway, NJ, USA: IEEE Press, 2025, pp. 1–4.
[23] Y. Jia, Z. Wang, C. Tang, L. Zhao, X. Li, and C. Wang, "An efficiency improvement method for the small air gap wireless power transfer system with variable parameters," *IEEE Trans. Power Electron.*, vol. 38, no. 11, pp. 13443–13453, Nov. 2023.
[24] G. Zhu, J. Dong, W. Shi, T. B. Soeiro, J. Xu, and P. Bauer, "A mode-switching-based phase shift control for optimized efficiency and wide ZVS operations in wireless power transfer systems," *IEEE Trans. Power Electron.*, vol. 38, no. 4, pp. 5561–5575, Apr. 2023.
[25] R. Ruffo, V. Cirimele, M. Diana, M. Khalilian, A. L. Ganga, and P. Guglielmi, "Sensorless control of the charging process of a dynamic inductive power transfer system with an interleaved nine-phase boost converter," *IEEE Trans. Ind. Electron.*, vol. 65, no. 10, pp. 7630–7639, Oct. 2018.
[26] "Infineon EVAL_1EDF_G1_HB_GAN webpage." Infineon. Accessed: Mar. 20, 2026. [Online]. Available: https://www.infineon.com/evaluation-board/EVAL-1EDF-G1-HB-GAN#documents
[27] C.-S. Wang, G. Covic, and O. Stielau, "Power transfer capability and bifurcation phenomena of loosely coupled inductive power transfer systems," *IEEE Trans. Ind. Electron.*, vol. 51, no. 1, pp. 148–157, Feb. 2004.
[28] J. Sallán, J. L. Villa, A. Llombart, and J. F. Sanz, "Optimal design of ICPT systems applied to electric vehicle battery charge," *IEEE Trans. Ind. Electron.*, vol. 56, no. 6, pp. 2140–2149, Jun. 2009.
[29] Y. Li et al., "Extension of ZVS region of series–series WPT systems by an auxiliary variable inductor for improving efficiency," *IEEE Trans. Power Electron.*, vol. 36, no. 7, pp. 7513–7525, Jul. 2021.
[30] Y. Mei, J. Wu, X. He, H. Zhang, and F. Lu, "Study on parasitic capacitance effect in high power inductive power transfer system," in *Proc. IEEE Energy Convers. Congr. Expo. (ECCE)*, 2019, pp. 129–134.
[31] C. R. Paul, R. C. Scully, and M. A. Steffka, *Introduction to Electromagnetic Compatibility*, 3rd ed. Hoboken, NJ, USA: Wiley, 2023.

Mattia Simonazzi (Member, IEEE) received the M.Sc. degree cum laude in electrical engineering in 2019 and the Ph.D. degree (Hons.) in biomedical, electrical, and system engineering in 2023, both from Alma Mater Studiorum – University of Bologna, Bologna, Italy. He is currently a Junior Assistant Professor with the Department of Electrical, Electronic, and Information Engineering "Guglielmo Marconi" with the University of Bologna. Since 2024, he has been a Professor of Electrical Engineering for the Bachelor's programs in Industrial Engineering and Mechatronics. Since 2017, he has also served as a Teaching Assistant for courses in Electromagnetics, Electrical Engineering, and Electromagnetic Compatibility (EMC). His research interests include wireless power transfer systems, the integration of superconducting cables into power grids, electromagnetic compatibility for industrial and automotive applications, and magnetic metamaterials. He is a Young Editorial Board Member of the journal Electricity. He has actively published in international journals and participated in several international conferences in the fields of electromagnetics, superconductivity, EMC, and power electronics, serving as speaker, tutorial presenter, and special session organizer.

Vincenzo Cirimele (Senior Member, IEEE) received the M.Sc. degree in electrical engineering (summa cum laude) in 2013 from the Politecnico di Torino, Turin, Italy, where he held the position of Assistant Professor with the Energy Department from 2017 to 2020. He received the Ph.D. degree in electronics engineering (with Hons.) from the Politecnico di Torino and in electrical engineering from the Université Paris-Saclay, France, in 2017. He is currently an Associate Professor with the Department of Electrical, Electronic, and Information Engineering, Alma Mater Studiorum, University of Bologna, Bologna, Italy. Since 2024, he has served as a Scientific Advisor for the company ENRX. His research interests include technologies for electric mobility, inductive power transmission, electromagnetic modeling and simulation, and power electronics. He acts as the Deputy Editor for *IET Power Electronics* and an Associate Editor for the journals IEEE TRANSACTIONS ON TRANSPORTATION ELECTRIFICATION and *Wireless Power Transfer*.

Riccardo Mandrioli (Senior Member, IEEE) received the Ph.D. degree (Hons.) in biomedical, electrical, and system engineering from the University of Bologna, Bologna, Italy, in 2023. He is currently a Tenure Track Assistant Professor (RTT) in electrical engineering, with the Department of Electrical, Electronic, and Information Engineering, University of Bologna. From 2022 to 2024, he has been a Postdoctoral Research Fellow and an Adjunct Professor, and he has also been involved as a Teaching Assistant for multiple engineering courses since 2017. In 2022, he was a Visiting Scientist with the Chair of Power Electronics, Kiel University, Kiel, Germany. In 2023, he received the National Scientific Habilitation (ASN) for the permanent position of Associate Professor in Electrical Engineering. His research interests include electric vehicle chargers, photovoltaic, power electronic converters, harmonic pollution, efficiency improvement, and circuit modeling. He was the winner of several awards with IEEE. He is an Associate Editor for IEEE ACCESS and an Editorial Board Member of several journals.

Leonardo Sandrolini (Senior Member, IEEE) received the Laurea (Hons.) and Ph.D. degrees in electrical engineering from Alma Mater Studiorum – Università di Bologna, Bologna, Italy, in 1995 and 2000, respectively. Since 2001, he has been with the Alma Mater Studiorum – Università di Bologna, where he is currently an Associate Professor with the Department of Electrical, Electronic, and Information Engineering "Guglielmo Marconi" (DEI). His teaching activities include courses in electrotechnics, electromagnetic compatibility and applied electromagnetics. His research interests include electromagnetic field theory, electromagnetic compatibility (shielding, electromagnetic coupling, conducted emissions, power quality, electromagnetic characterisation of dispersive materials, electromagnetic interference in switching converters, electromagnetic interference in railways), electrical characterisation of renewable energy sources, and wireless power transfer with resonant inductive coupling. He has authored or coauthored approximately 150 papers in peer-reviewed international journals and conference proceedings and holds two patents. He is an Associate Editor of the Wiley journals *International Journal of Photoenergy* and *International Journal of RF and Microwave Computer-Aided Engineering*, and of the *MDPI Journal Electronics*. He is also a member of the Advisory Board of Elsevier journal *International Journal of Electrical Power & Energy Systems*. He is a member of the IEEE EMC Society TC 7 Electrical Systems and Power Electronics EMC and the IEEE MTT Society TC MTT-26 Wireless Energy Transfer and Conversion.

Open Access funding provided by 'Universita di Bologna' within the CRUI CARE Agreement